

Separating the bulk and interface contribution of spin-orbit torque in ferromagnet-Heavy metal bilayers tuned by variation of resistivity of heavy metal

Abu Bakkar Miah, Dhananjaya Mahapatra, Soumik Aon, Harekrishna Bhunia, and Partha Mitra

Department of Physical Sciences, Indian Institute of Science Education and Research Kolkata, Mohanpur, West Bengal, 741246, INDIA.

(*1pmitra@iiserkol.ac.in)

(*1abm17rs055@iiserkol.ac.in)

(Dated: March 10, 2025)

Harmonic Hall measurements were conducted on a series of Ferromagnetic metal/Heavy metal (FM/HM) bilayers with β -Tungsten (W) as the HM and in-plane magnetized permalloy (Py) as the FM and the efficiencies of the two orthogonal components of the spin orbit-torque were extracted. Two sets of Hall bar-shaped devices were considered where the HM resistivity systematically varied over a wide range (~ 150 - $1000 \mu\Omega$ -cm) while the FM layer remained the same and each set having a different aspect ratio of voltage pickup line width and Hall bar width. Using numerical simulations of current distribution at the region between voltage pickup lines we have normalised the SOT efficiencies and examined their dependence. The current-induced spin-orbit torque efficiency (ξ) in ferromagnetic metal (FM)/heavy metal (HM) bilayers is quantitatively investigated in this study. β -W, known for its high spin-orbit coupling, served as the HM layer, while Py, an FM with an in-plane magnetic anisotropy, comprised the other layer. We performed a thorough analysis of the second harmonic Hall resistance ($R_{xy}^{2\omega}$) obtained from Py/ β -W bilayer devices, systematically varying the resistivity (ρ_W) of the β -W layer within the range of 200 to 1000 $\mu\Omega$ -cm by employing a fixed current density ($J_W \sim 0.8 \times 10^{11} A/m^2$) through β -W. Through this analysis, we derived the Slonczewski-like efficiency (ξ_{SL}) and field-like efficiency (ξ_{FL}) as a function of ρ_W . Notably, the device with a resistivity of 980 $\mu\Omega$ -cm exhibited the highest ξ_{SL} , yielding a value of -0.42 ± 0.09 . These results highlight the promising potential of highly resistive β -W as a material of interest in spintronics research. Specifically, it shows promise in enhancing the performance of magnetic sensing devices, thereby contributing to advancements in spintronic applications.

A bilayer comprising a ferromagnetic metal (FM) and a heavy metal (HM) has proven to be a simple yet effective platform for experimentally verifying fundamental concepts in spinorbitronics. HM is a generic term used to denote conductors with strong spin-orbit coupling (SOC) strength e.g. large atomic weight elemental metals, topological insulators, semiconductors etc. A typical signature of HMs is the presence of a measurable spin Hall effect (SHE)[1–4], due to which a transverse pure spin current is generated in response to an applied charge current. This spin current is absorbed by the magnetization of the adjacent FM layer, playing a crucial role in the magnetization dynamics, referred to as spin-orbit torque (SOT)[5–14]. In addition to SHE-induced spin current which is controlled by the bulk properties of the HM, SOT can also arise from the Rashba-Edelstein Effect (REE) [15, 16] which is due to the FM/HM interface properties. When a charge current flows parallel to an interface, it acquires a net spin accumulation at the interface where inversion symmetry is broken. concurrently, a transverse electric field (E_R) is generated at the interface between two different metals, which is perpendicular to the plane and the direction of the charge current[15]. This spin accumulation can exert torque on an adjacent ferromagnet through the transfer of spin angular momentum[11, 15, 17–20]. Both experimentally and theoretically, it has been established that there are two types of induced magnetic fields generated by spin accumulation at the interface. These fields are mutually perpendicular to each other and to the magnetization of the FM. For in-plane magnetization systems, the field-like(FL) field ($\vec{B}_{FL} \sim \hat{\sigma}$) acts in-plane, while the Slonczewski-Like (SL) field ($\vec{B}_{SL} \sim \hat{m} \times \hat{\sigma}$) acts out of plane. The corresponding FL torque ($\vec{\tau}_{FL} \sim \hat{m} \times \hat{\sigma}$) acts out of plane, and the SL torque ($\vec{\tau}_{SL} \sim$

$\hat{m} \times (\hat{m} \times \hat{\sigma})$) acts in-plane, where \hat{m} is the magnetization unit vector, and $\hat{\sigma}$ is the unit vector along the spin polarization direction. SL torque originates from bulk SHE inside a heavy metal with a thickness sufficiently larger than the spin diffusion length (λ_s)[19]. Recently, a large ξ_{SL} has been reported in bilayers containing β -W[14, 21–25], Pt[10, 13, 20, 26], and β -Ta[26, 27], among which β -W is considered a leading candidate for applications due to its large SOC. Moreover, ξ_{SL} can be enhanced by increasing the resistivity of W. Motivated by Zhang et al. [25] proposal, we present a systematic study on the harmonic Hall measurements of Py/ β -W bilayer Hall-bar structures, featuring a wide range of resistivity values for Py/ β -W films, ranging from 200 to 1000 $\mu\Omega$ -cm. We aim to enhance the ξ_{SL} by increasing the resistivity ρ_W . Additionally, we investigated the impact of thermally driven effects and the Oersted field (B_{Oe}) in our SOT measurements. Our measurements and analyses shed light on the influence of the SOT behavior in the Py/ β -W bilayer system with ρ_W .

A series of Py(6)/ β -W(15) devices with an aspect ratio of 0.26 were fabricated on Si/SiO₂ (300 nm) substrates at room temperature. Electron beam lithography was performed to pattern all Hallbar devices ($2 \times 20 \mu m^2$). The Py film was deposited onto the Hallbar patterned substrates using thermal evaporation with a deposition rate of (0.3-0.4) Å/sec under a base pressure $\sim 10^{-7}$ Torr. Subsequently, β -W film was deposited on Py utilizing DC magnetron sputtering. A low deposition rate was maintained to promote the formation of the β -phase of W. The deposition was carried out at a controlled rate of (0.4-0.3) Å/sec. Concurrently, the Ar pressure was varied within a range of 4.5 to 8 mTorr during the deposition process. Additionally, Optical lithography was performed to pattern the contact pads. Finally, Cr(5)/Au(30) con-

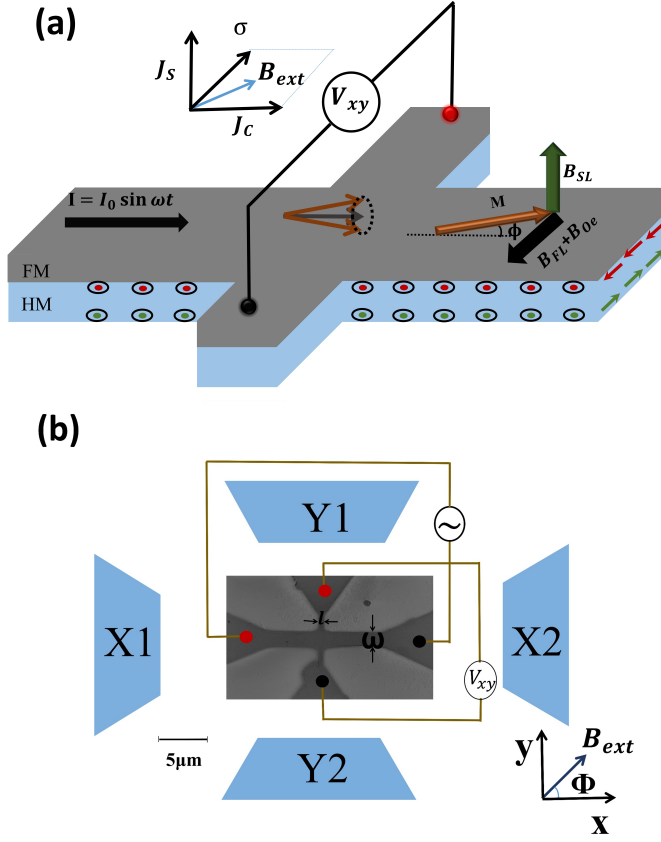


FIG. 1. (a) Schematic cartoon represents a Hallbar, where a charge current (J_C) creates the spin current (J_S) and J_S contributes to the magnetization dynamics in Py, (red and green arrows) represents the spin polarization direction σ , and (b) Schematic of the measurement setup consisting of an SEM image of the device and electromagnet pole pieces (X1, X2, Y1, and Y2), red and black circles represent the positive and negative terminals of electrical connection.

tact pads were deposited using electron beam evaporation. Ar ion milling was performed before all depositions to clean the interfaces and enhance film quality. The room temperature resistivity of all β -W (ρ_W) and Py (ρ_{Py}) films was measured using the standard Van der Pauw (VDP) method. The obtained ρ_W values for the β -W films were found to be 218, 290, 454, 800, and 980 $\mu\Omega$ -cm, respectively, while the ρ_{Py} value for the Py film was measured to be 250 $\mu\Omega$ -cm. Surface roughness measurements of the films were performed using atomic force microscopy (AFM), obtaining a roughness value ~ 0.2 nm for β -W and ~ 0.1 nm for Py film.

The second harmonic transverse hall measurement is a technique used to separate the SL and FL contributions of SOT[28]. The application of an AC charge current generates an oscillating spin current, which influences the magnetization oscillation. This process leads to the observation of transverse second-harmonic resistance. In-plane transverse harmonic Hall measurements were performed using an SR830 lock-in amplifier in conjunction with a Keithley 6221 AC and

DC source. An AC (I) was applied along the x-direction, and the transverse resistance was measured in the y-direction, as illustrated in Fig.1(a). The angle between I and B_{ext} is ϕ . To investigate the influence of B_{ext} on the sample, two distinct types of measurements were conducted: (a) B_{ext} (300mT to 10mT) was fixed while taking $\phi = 0^\circ$ to 360° rotation in the sample plane, and (b) In the second set of measurements, the B_{ext} was swept in the sample plane over a range, varying from 400 mT to -400 mT and B_{ext} was maintained at fixed angles of $\phi=45^\circ, 135^\circ, 225^\circ$ and 315° during this process. A customized sample holder was employed to securely place the sample inside the pole pieces of the electromagnet. This arrangement ensured proper alignment and stability during the measurements. All measurements were carried out at room temperature, and the frequency of the applied AC was maintained at 13Hz throughout the measurement process. We employed a well-defined measurement setup, the schematic diagram of the device depicted in FIG.1(b).

In the transverse harmonic Hall measurement, the first harmonic signal provided valuable information regarding the direction of the magnetization at equilibrium. On the other hand, the second harmonic signal revealed the perturbative tilting of the magnetization induced by SOT[29]. When current I is applied along x, it is divided between the W and Py layers according to their respective resistivities. The parallel-circuit model is applied to determine the current density flowing in the W and Py layers. current density in W and Py can be written as,

$$J_W = \frac{I}{(\omega_W t_W) [1 + (\frac{\rho_W}{\rho_{Py}}) (\frac{t_{Py}}{t_W})]}$$

and

$$J_{Py} = \frac{(\frac{\rho_W}{\rho_{Py}}) (\frac{t_{Py}}{t_W}) I}{(\omega_{Py} t_{Py}) [1 + (\frac{\rho_W}{\rho_{Py}}) (\frac{t_{Py}}{t_W})]}$$

Throughout the measurement, we have maintained a fixed $J_W = 0.8 \times 10^{11} A/m^2$. Current-induced effective fields (B_{SL} and B_{FL}) induce periodic oscillations on the magnetization around its equilibrium position. The first harmonic Hall resistance measurement is equivalent to the DC resistance measurement (external magnetic field, B_{ext} or time-independent) but the higher harmonic signals are strongly dependent on B_{ext} . For small oscillations of the magnetization, the Hall resistance $R_{xy}(t)$ can be expanded up to the first order[29]. This expansion allows for the characterization of the sample's magnetic properties and the determination of the strength and behavior of B_{SL} and B_{FL} . By analyzing the first harmonic and second harmonic responses, valuable information about the SOT effects can be obtained. The expressions for 1ω and 2ω resistances can be represented as [24, 30–36]...

$$R_{xy}^\omega = R_{PHE} \sin(2\phi) \quad (1)$$

and

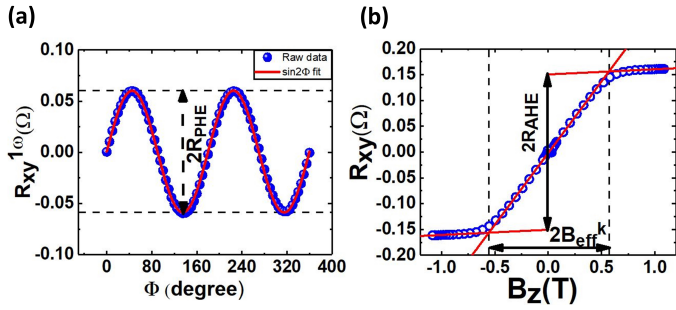


FIG. 2. (a) First harmonic Hall resistance ($R_{xy}^{1\omega}$) vs in-plane rotation of the magnetic field of Py/ β -W218 device, fitted with the equation. (1). (b) Anomalous Hall signal of Py/ β -W218 device. The intersection between low and high field fitted lines gives the value of B_{eff}^k .

$$R_{xy}^{2\omega} = \left[-R_{AHE} \left(\frac{B_{SL}}{B_{ext} + B_{eff}^k} \right) + \alpha B_{ext} + R_{\Delta T}^0 \right] \cos\phi + 2R_{PHE} \left(\frac{B_{FL} + B_{Oe}}{B_{ext}} \right) \cos 2\phi \cos\phi + R_{PNE} \sin 2\phi \quad (2)$$

Where, R_{AHE} is the anomalous Hall resistance, B_{Oe} is the Oersted field, B_{eff}^k is the effective anisotropy field, R_{PHE} is the planar Hall amplitude, ϕ is the angle between magnetization and current, α is the ordinary Nernst (ONE) co-efficient, $R_{\Delta T}^0$ is the anomalous Nernst (ANE) co-efficient and R_{PNE} is the planar Nernst coefficient.

To analyze the SOT effects, the values of R_{AHE} and B_{eff}^k are essential parameters. The values of R_{AHE} and B_{eff}^k were obtained through an out-of-plane magnetic field (B_z) sweep spanning a range from +1.1 T to -1.1T. FIG.2(b) displays typical experimental data of Hall resistance (R_{Hall}) plotted against the B_z . To extract any effects resulting from field misalignment, the data was antisymmetrized. By performing a linear fit to the high-field region, the value of R_{AHE} was extracted. Simultaneously, the interception of low-field region and high-field region linear fit provided the value of B_{eff}^k . The obtained values of B_{eff}^k range from 0.45 to 0.59T and exhibit no pronounced trend concerning ρ_W [24]. On the other hand, the R_{PHE} value was determined by fitting the first harmonic data with equation 7, as shown in FIG.2(a).

we have shown 2ω signal for two different (30mT and 100mT) magnetic fields in FIG.3 and from there we can say that the oscillations of 2ω signal suppress by the increase of the value of B_{ext} . Symmetrized all 2ω data concerning $\phi = 180$. To extract the $\cos\phi$ contribution from the symmetrized signal, four data points for angles $\phi=45^\circ$, 135° , 225° and 315° has taken and a $\cos\phi$ curve was fitted through the four signal values, as shown in Fig.3(b). Subsequently, the fitted $\cos\phi$ curve was subtracted from the symmetrized 2ω signal, effectively removing the $\cos\phi$ contribution. This subtraction resulted as $\cos 2\phi \cos\phi$ contribution, shown in Fig.3(c). In our study, we conducted measurements of the angular variation (0° to 360°) of 2ω signal under different magnetic fields, ranging from $B_{ext} = 10$ mT to 300 mT. The experimental data

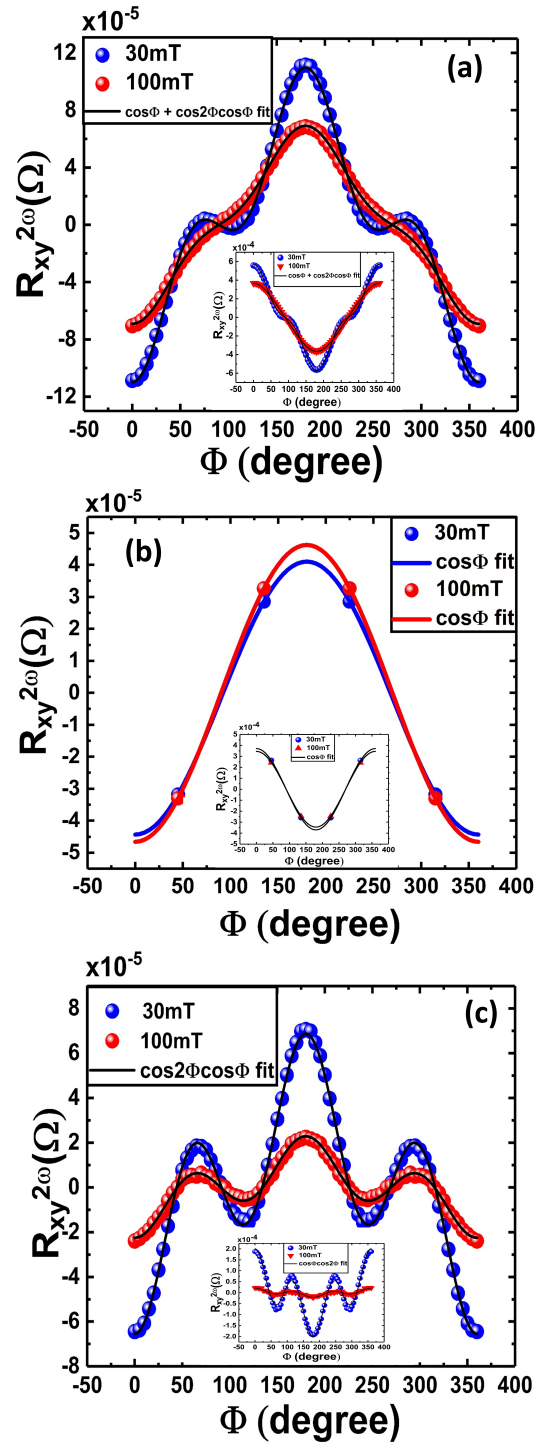


FIG. 3. (a) Second harmonic Hall resistance ($R_{xy}^{2\omega}$) vs in-plane rotation of the magnetic field, at low and high external magnetic fields for Py/W218 device, in the inset a Py/Pt data has shown to visualize the opposite qualitative behavior, (b) $\cos\phi$ contribution of $R_{xy}^{2\omega}$, and (c) $\cos(2\phi)\cos(\phi)$ contribution after subtracting $\cos(\phi)$ contribution from the symmetrized 2ω signal.

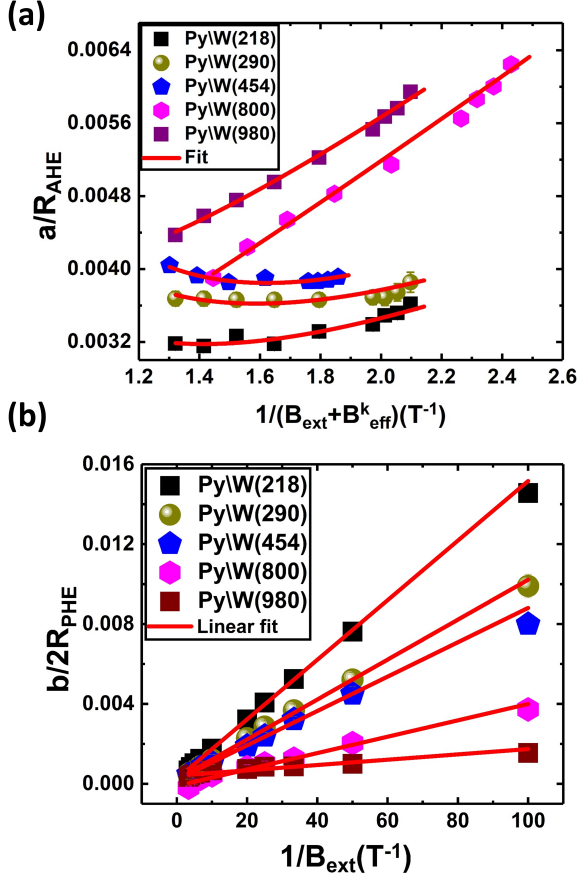


FIG. 4. (a) Co-efficient of $\cos(\phi)$ of second harmonic signal a vs $\frac{1}{(B_{ext} + B_{eff}^k)}$ and solid lines are fit with equation.4, (b) Co-efficient of $\cos(2\phi)\cos(\phi)$ 'b' vs $\frac{1}{B_{ext}}$.

was then fitted with a symmetrized form of equation.2 in the form of:

$$R_{xy}^{2\omega} = a \cos\phi + b \cos 2\phi \cos\phi \quad (3)$$

After the fit, we obtained the corresponding values of a and b for each magnetic field. These parameters are related to the physical properties of the sample, and they are given by:

$$a = \left[-R_{AHE} \left(\frac{B_{SL}}{B_{ext} + B_{eff}^k} \right) + \alpha B_{ext} + R_{\Delta T}^0 \right] \quad (4)$$

and

$$b = 2R_{PHE} \left(\frac{B_{FL} + B_{Oe}}{B_{ext}} \right) \quad (5)$$

To isolate the B_{SL} term from a , we plotted $\frac{a}{R_{AHE}}$ vs $\frac{1}{B_{ext} + B_{eff}^k}$ and performed a non-linear fit with the form $cx + d(1/x - B_{eff}^k) + e$. The value of c from the fit represents the value of $-B_{SL}$. Similarly, to isolate the B_{FL} term from b we plotted $\frac{b}{2R_{PHE}}$ vs $\frac{1}{B_{ext}}$ and performed a linear fit. The slope gives the

value of $B_{FL} + B_{Oe}$. The value obtained for $B_{FL} + B_{Oe}$ represents the combined effect of B_{FL} and B_{Oe} . From Ampere's circuital law $B_{Oe} = \frac{\mu_0 I_W}{2w}$ is calculated. Additionally, ANE and ONE coefficients can be extracted during the fitting process.

In FIG.3(a), We observe a transition in a vs $\frac{1}{(B_{ext} + B_{eff}^k)}$ plot when ρ_W goes from $454 \mu\Omega\text{-cm}$ to $800 \mu\Omega\text{-cm}$. This is the transition from the mixed $(\alpha + \beta)$ -phase to pure β -phase of W, further confirmed by the XRD analysis. The efficiency of SOT for FM/HM bilayer under a current density J_{HM} is characterized by[27, 37]:

$$\xi_{SL(FL)} = \frac{2e}{\hbar} \frac{B_{SL(FL)} M_s t_{FM}}{J_{HM}} \quad (6)$$

where e , \hbar , M_s , $B_{SL(FL)}$, t_{FM} , and J_{HM} are the electronic charge, reduced Planck's constant, saturation magnetization, induced SL(FL) fields, the thickness of the FM, and current density flowing through the heavy metal layer respectively. The value of $M_s = 7.16 \times 10^5 \text{ A/m}$ for a 6 nm thick Py film is obtained from the demagnetization field (B_{dem}). The SL efficiency in terms of spin Hall conductivity (σ_{SH}), resistivity of W (ρ_W) and the spin mixing conductance ($G^{\uparrow\downarrow}$) approximately as for $t_W \gg \lambda_s$ [38]

$$\xi_{SL} = \frac{\frac{2e}{\hbar} \sigma_{SH} (2\lambda_s G_r) \rho_W^2}{1 + 2\lambda_s G_r \rho_W} \quad (7)$$

where G_r is the real part of the spin mixing conductance $G^{\uparrow\downarrow} = G_r + iG_i$ and we have assumed $G_r \gg G_i$, and from that we get, ρ_W^2 / ξ_{SL} has the linear dependency on ρ_W . From the linear fit, we obtained the values of $G_r \approx 1 \times 10^{14} \Omega^{-1} m^{-2}$ [38] and $\sigma_{SH} \approx 0.42 \times 10^5 (\frac{\hbar}{2e}) \Omega^{-1} m^{-1}$ [39] by putting spin diffusion length of W, $\lambda_s = 2.575 \text{ nm}$. Further, we have calculated the Rashba constant (α_R) to check the strength of the REE from the expression[38].

$$\alpha_R = \frac{2\mu_B M_s B_{FL}}{P J_W} \quad (8)$$

Where μ_B and P are the Bohr Magneton and spin polarization of the FM respectively, it ranges from 0.0224 to 0.0304 for the given range of ρ_W and the obtained values are relatively smaller than the previous study on 2D systems[40].

In our experimental study, we analyzed the $R_{xy}^{2\omega}$ signals and separated the SL and FL contributions, obtaining the corresponding SOT efficiencies (ξ_{SL} and ξ_{FL}). We employed a fixed current density $J_W \sim 0.8 \times 10^{11} \text{ A/m}^2$ for all bilayer devices. The values of ξ_{SL} are found to be -0.26, -0.30, -0.37, -0.41, and -0.42 for five devices in our study with an aspect ratio ($\frac{L}{w}$) 0.26. We found that the SL efficiency is more significant in high-resistive β -W devices, the highest observed value is -0.42 ± 0.09 for $980 \mu\Omega\text{-cm}$ device. Similarly, the ξ_{FL} values are from -0.107 to -0.146. These results suggest that more spin current is generated in high-resistive β -W (pure β phase) films. Nevertheless, we have done the same measurement on a different set of devices with an aspect ratio of 0.71 and analyzed the data and the two sets of results do not match, as shown in FIG.5(a) and (b). We know $V_{2\omega} \sim J_x^2$, J_x varies

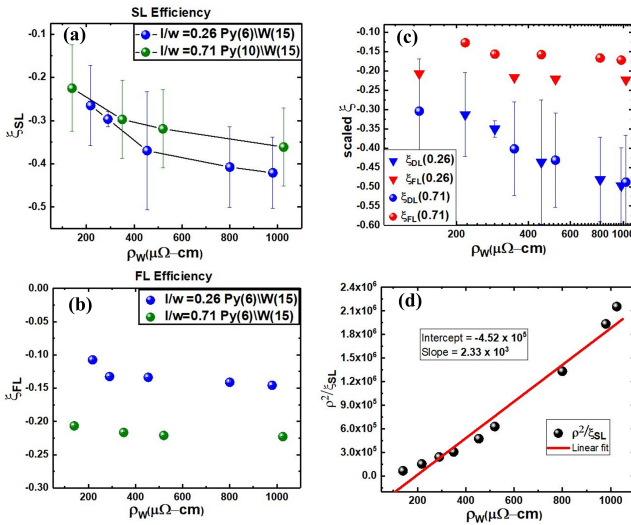


FIG. 5. (a) and (b) are the ξ_{SL} and ξ_{FL} vs resistivity plot of two sets of devices with an aspect ratio 0.26 (blue spheres) and 0.71 (green spheres), (c) represents the scaled ξ_{SL} and ξ_{FL} of two sets of devices vs resistivity, and (d) ρ^2/ξ_{SL} vs ρ_W fitted with a straight line.

with the aspect ratio which means 2ω signal depends on the current density at the center of the Hallbar. To conclude this,

we have measured a series of devices by varying the aspect ratio from 0.125 to 1.25 and getting a SOT efficiency variation. From this, we take SOT efficiencies corresponding to 0.26 and 0.71 aspect ratios and scale the efficiencies of two sets of devices with the mentioned aspect ratio and interestingly ξ_{SL} for both sets match well, whoever ξ_{FL} has a clear shift. The reason could be the resistivity of the ferromagnet, two sets have different resistivity of Py and it can create different polarisation values of the ferromagnet. While analyzing our data, we noted the emergence of an asymmetric component within the 2ω signal. This asymmetry could stem from factors including sample misalignment relative to the magnetic field, deviations in Hall branches alignment, drift, and in-plane temperature gradients. Notably, these asymmetrical signals were of minor significance, merely 8 to 10 percent of the symmetric signal, which is also consistent with Avci et al.[28]. Aoki et al. represent this signal as a planar Nernst signal for Weyl ferromagnet Co_2MnGa which is proportional to $\sin 2\phi$ [36]. From the ξ_{SL} vs ρ_W plot, we observe a systematic enhancement of the SOT efficiencies with resistivity, which indicates that more spin current is generated in high resistive W and it is creating more SOT on the magnetization of the ferromagnet. These findings shed light on the correlation between the resistivity of W and SOT efficiency, suggesting the potential for tailoring the SOT efficiency by controlling the resistivity of the W films.

-
- [1] M. I. D'Yakonov and V. I. Perel', Soviet Journal of Experimental and Theoretical Physics Letters **13**, 467 (1971).
- [2] J. E. Hirsch, Phys. Rev. Lett. **83**, 1834 (1999).
- [3] S. Zhang, Phys. Rev. Lett. **85**, 393 (2000).
- [4] J. Sinova, D. Culcer, Q. Niu, N. A. Sinitsyn, T. Jungwirth, and A. H. MacDonald, Phys. Rev. Lett. **92**, 126603 (2004).
- [5] A. Manchon and S. Zhang, Phys. Rev. B **78**, 212405 (2008).
- [6] A. Manchon and S. Zhang, Phys. Rev. B **79**, 094422 (2009).
- [7] A. Matos-Abiague and R. L. Rodríguez-Suárez, Phys. Rev. B **80**, 094424 (2009).
- [8] D. A. Pesin and A. H. MacDonald, Phys. Rev. B **86**, 014416 (2012).
- [9] A. Chernyshov, M. Overby, X. Liu, J. Furdyna, Y. Lyanda-Geller, and P. Leonid, Nature Physics **5**, 9 (2009).
- [10] I. Miron, G. Gaudin, S. Auffret, B. Rodmac, A. Schuhl, S. Pizzini, J. Vogel, and P. Gambardella, Nature materials **9**, 3 (2010).
- [11] I. Miron, K. Garello, G. Gaudin, P. Zermatten, M. Costache, S. Auffret, S. Bandiera, B. Rodmac, A. Schuhl, and P. Gambardella, Nature **476**, 7359 (2011).
- [12] K. Ando, S. Takahashi, K. Harii, K. Sasage, J. Ieda, S. Maekawa, and E. Saitoh, Phys. Rev. Lett. **101**, 036601 (2008).
- [13] L. Liu, T. Moriyama, D. C. Ralph, and R. A. Buhrman, Phys. Rev. Lett. **106**, 036601 (2011).
- [14] M. Cubukcu, O. Boulle, M. Drouard, K. Garello, C. Onur Avci, I. Mihai Miron, J. Langer, B. Ocker, P. Gambardella, and G. Gaudin, Applied Physics Letters **104**, 042406 (2014).
- [15] V. Edelstein, Solid State Communications **73**, 233 (1990).
- [16] S. D. Ganichev, V. V. Bel'kov, L. E. Golub, E. L. Ivchenko, P. Schneider, S. Giglberger, J. Eroms, J. De Boeck, G. Borghs, W. Wegscheider, D. Weiss, and W. Prettl, Phys. Rev. Lett. **92**, 256601 (2004).
- [17] P. Gambardella and I. M. Miron, Philosophical Transactions of the Royal Society A: Mathematical, Physical and Engineering Sciences **369**, 3175 (2011).
- [18] T. D. Skinner, M. Wang, A. T. Hindmarch, A. W. Rushforth, A. C. Irvine, D. Heiss, H. Kurebayashi, and A. J. Ferguson, Applied Physics Letters **104**, 062401 (2014).
- [19] M. Kawaguchi, T. Moriyama, T. Koyama, D. Chiba, and T. Ono, Journal of Applied Physics **117**, 17C730 (2015).
- [20] G. Allen, S. Manipatruni, D. E. Nikonov, M. Doczy, and I. A. Young, Phys. Rev. B **91**, 144412 (2015).
- [21] Q. Hao, W. Chen, and G. Xiao, Applied Physics Letters **106**, 182403 (2015).
- [22] C.-F. Pai, L. Liu, Y. Li, H. W. Tseng, D. C. Ralph, and R. A. Buhrman, Applied Physics Letters **101**, 122404 (2012).
- [23] C.-F. Pai, M.-H. Nguyen, C. Belvin, L. H. Vilela-Leão, D. C. Ralph, and R. A. Buhrman, Applied Physics Letters **104**, 082407 (2014).
- [24] Y. Takeuchi, C. Zhang, A. Okada, H. Sato, S. Fukami, and H. Ohno, Applied Physics Letters **112**, 192408 (2018).
- [25] C. Zhang, S. Fukami, K. Watanabe, A. Ohkawara, S. DuttaGupta, H. Sato, F. Matsukura, and H. Ohno, Applied Physics Letters **109**, 192405 (2016).
- [26] Y.-C. Lau and M. Hayashi, Japanese Journal of Applied Physics **56**, 0802B5 (2017).
- [27] A. V. Khvalkovskiy, V. Cros, D. Apalkov, V. Nikitin, M. Krounbi, K. A. Zvezdin, A. Anane, J. Grollier, and A. Fert, Phys. Rev. B **87**, 020402 (2013).
- [28] C. O. Avci, K. Garello, M. Gabureac, A. Ghosh, A. Fuhrer, S. F. Alvarado, and P. Gambardella, Phys. Rev. B **90**, 224427

- (2014).
- [29] E.-S. Park, D.-K. Lee, B.-C. Min, and K.-J. Lee, *Phys. Rev. B* **100**, 214438 (2019).
- [30] R. Itoh, Y. Takeuchi, S. DuttaGupta, S. Fukami, and H. Ohno, *Applied Physics Letters* **115**, 242404 (2019).
- [31] K. Vihanga De Zoysa, S. DuttaGupta, R. Itoh, Y. Takeuchi, H. Ohno, and S. Fukami, *Applied Physics Letters* **117**, 012402 (2020).
- [32] L. Zhu, X. Xu, T. Zhang, M. Wang, K. Meng, Y. Wu, J. Chen, and Y. Jiang, *Applied Physics Letters* **120**, 252404 (2022).
- [33] C. Yang, C. Egecan, R. D. Resnick, J. J. Michel, N. N. Statuto, A. Kent, and F. Yang, *Nature Communications* **13**, 3659 (2022).
- [34] N. Roschewsky, E. S. Walker, P. Gowtham, S. Muschinske, F. Hellman, S. R. Bank, and S. Salahuddin, *Phys. Rev. B* **99**, 195103 (2019).
- [35] J. U. Ahn, J. Jeon, S. W. Cho, O. Lee, S. Lee, and H. C. Koo, *Current Applied Physics* **49**, 12 (2023).
- [36] M. Aoki, Y. Yin, S. Granville, Y. Zhang, N. V. Medhekar, L. Leiva, R. Ohshima, Y. Ando, and M. Shiraishi, *Nano Letters* **23**, 6951 (2023).
- [37] C.-F. Pai, Y. Ou, L. H. Vilela-Leão, D. C. Ralph, and R. A. Buhrman, *Phys. Rev. B* **92**, 064426 (2015).
- [38] P. M. Haney, H.-W. Lee, K.-J. Lee, A. Manchon, and M. D. Stiles, *Physical Review B* **87**, 174411 (2013).
- [39] H. Wang, C. Du, Y. Pu, R. Adur, P. C. Hammel, and F. Yang, *Physical review letters* **112**, 197201 (2014).
- [40] A. Varykhalov, J. Sánchez-Barriga, A. Shikin, W. Gudat, W. Eberhardt, and O. Rader, *Physical review letters* **101**, 256601 (2008).
- [41] V. Tshitoyan, C. Ciccirelli, A. P. Mihai, M. Ali, A. C. Irvine, T. A. Moore, T. Jungwirth, and A. J. Ferguson, *Phys. Rev. B* **92**, 214406 (2015).
- [42] X. Luo, X. Wang, J. Wei, W. Yang, M. Zhao, Y. Wang, Y. Wang, W. He, B. He, Z. Zeng, C. Wan, X. Han, and G. Yu, *Phys. Rev. Appl.* **19**, 034043 (2023).
- [43] L. Neumann and M. Meinert, *AIP Advances* **8**, 095320 (2018).
- [44] J. Hidding, S. H. Tirion, J. Momand, A. Kaverzin, M. Mostovoy, B. J. V. Wees, B. J. Kooi, and M. H. D. Guimarães, *Journal of Physics: Materials* **4**, 04LT01 (2021).
- [45] Q. Hao and G. Xiao, *Phys. Rev. Appl.* **3**, 034009 (2015).